Spectral BRDF measurements of metallic samples for laser processing applications

2015 J. Phys.: Conf. Ser. 655 012064

(http://iopscience.iop.org/1742-6596/655/1/012064)

Journal of Physics: Conference Series **655** (2015) 012064 doi:10.1088/1742-6596/655/1/012064

Spectral BRDF measurements of metallic samples for laser processing applications

L Vitali, D Fustinoni, P Gramazio and A Niro
Politecnico di Milano, Department of Energy,
Campus Bovisa, Via Lambruschini 4, 20156 Milano, Italy

Corresponding author email: alfonso.niro@polimi.it

Abstract. The spectral bidirectional reflectance distribution function (BRDF) of metals plays an important role in industrial processing involving laser-surface interaction. In particular, in laser metal machining, absorbance is strongly dependent on the radiation incidence angle as well as on finishing and contamination grade of the surface, and in turn it can considerably affect processing results. Very recently, laser radiation is also used to structure metallic surfaces, in order to produce many particular optical effects, ranging from a high level polishing to angular color shifting. Of course, full knowledge of the spectral BRDF of these structured layers makes it possible to infer reflectance or color for any irradiation and viewing angles. In this paper, we present Vis-NIR spectral BRDF measurements of laser-polished metallic, opaque, flat samples commonly employed in such applications. The resulting optical properties seem to be dependent on the atmospheric composition during the polishing process in addition to the roughness. The measurements are carried out with a Perkin Elmer Lambda 950 double-beam spectrophotometer, equipped with the Absolute Reflectance/Transmittance Analyzer (ARTA) motorized goniometer.

1 Introduction

Laser surface processing techniques on metals are a subject of great interest from both a scientific and industrial standpoint, since they can allow faster machining times and yield more precise finishing properties than the mechanical counterpart. Moreover, they can be used to obtain several number of interesting features, like controlled microstructures for enhancing glues adhesion [1], coloring via oxidation phenomena, and surface polishing. However, laser machining requires the fine adjustment of several parameters, i.e., beam power, velocity and frequency, atmosphere composition and angle of incidence. Hence most of the works in open literature are about finding general correlations between the aforementioned parameters and the experimental results. In this context, the paper by Veiko et al. [2] proposes a correlation between a chromaticity coefficient and laser treatment regimes for stainless steel and titanium coloring, while the work by Bordatchev et al. [3] is an interesting review of laser polishing experiments on various metal surfaces carried out by several research groups, but the comparison takes into account only the starting and the achieved average roughness. The assessment of laser polishing processes requires a detailed optical surface characterization to define the visual appearance of the finished product, as well as to evaluate its radiative properties in engineering applications. Although the BRDF is only one of the parameters considered in [4] to evaluate visual appearance, where texture properties have to be taken into account, it still is the main measurable feature in characterizing surfaces, and it can give a full insight on the optical properties of a surface finish.

In this paper, Vis-NIR BRDF measurements are carried out on four laser polished steel samples, machined with two different sets of laser parameters in two different atmospheric compositions. The achieved optical properties are compared with those of the untreated steel, to show the effect of the laser surface processing.

2 Experiments

2.1 Spectral BRDF

The definition of BRDF, or f_r, for an element of area dA, has been given by Nicodemus et al. [5] as

$$f_r(\theta_i, \varphi_i; \theta_r, \varphi_r) = \frac{dL_r(\theta_i, \varphi_i; \theta_r, \varphi_r)}{dE_i(\theta_i, \varphi_i)} \quad [sr^{-1}] \tag{1}$$

where dL_r is the reflected radiance, dE_i is the incident irradiance, the spherical coordinates (θ_i,φ_i) and (θ_r,φ_r) are the generic directions of the incoming and the reflected radiation, respectively. This definition is valid under the assumption of geometrical (ray) optics, flat reference surface uniformly irradiated, and scattering properties uniform and isotropic across the reference plane.

Although BRDF is defined as a differential quantity, the use of finite quantities is needed for a definition of BRDF that can be applied in real measurement situations, typically with the rotation of the sample along one or two axes and a movable detector with an aperture area A_d that can revolve around the test object. Under these approximations, we get [6]

$$f_r(\theta_i, \varphi_i; \theta_r, \varphi_r) \approx \frac{L_r(\theta_i, \varphi_i; \theta_r, \varphi_r)}{E_i(\theta_i, \varphi_i)} = \frac{\Phi_r}{\Phi_i} \frac{r^2}{\cos(\theta_r) A_d} \quad [sr^{-1}] \tag{2}$$

where Φ_i and Φ_r are the incident and reflected fluxes, respectively, r is the center to center distance from the sample to detector aperture. However, f_r is a total quantity whereas for our purposes, where fluorescence effects are absent and the wavelength of the incident and reflected radiation is the same, we introduce a spectral BRDF $f_{r,\lambda}$, defined by similarity with equation (2) as

$$f_{r,\lambda}(\theta_i, \varphi_i; \theta_r, \varphi_r; \lambda) \approx \frac{L_{r,\lambda}(\theta_i, \varphi_i; \theta_r, \varphi_r, \lambda)}{E_{i,\lambda}(\theta_i, \varphi_i, \lambda)} = \rho(\lambda) \frac{r^2}{\cos(\theta_r) A_d} \quad [sr^{-1}] \tag{3}$$

where $\rho(\lambda)$ is the measured spectral reflectance for a given direction of incident radiation and for a given detector position, i.e. the $\Phi_{r,\lambda}(\lambda)$ to $\Phi_{i,\lambda}(\lambda)$ ratio.

2.2 Geometric definitions

With respect to the geometry of the experimental apparatus that will be introduced in the next paragraph, let us define a few relevant angles, which are also visualized in figures 1 and 2. Given a specimen whose test surface lays on the x-y plane, and being the z axis coincident with its normal direction, in our configuration the incident and reflected beams lay always on the x-z plane, thus the azimuth angle φ is always 0. Three angles define the geometry of the setup for a single spectrophotometric measure, namely the incidence angle θ_i, between the incident beam and the sample normal, positive clockwise, the detector angle θ_d, between the incident beam and the line joining the detector and sample centers, positive clockwise, and the aspecular angle θ_a, defined as the angle from direct specular direction, positive towards incident illumination. In particular, the relationship between these three angles is expressed in equation 4:

$$\theta_a = 2\theta_i - \theta_d \tag{4}$$

being $2\theta_i$ the angle between incident and specular reflected radiation. θ_d is the angular position of the detector that collects the reflected radiation, hence it corresponds to θ_r in the BRDF definition given by equation (3). The range of the angles is from 10° to 350° for θ_d, although the extremities shouldn't be reached because the beam periscope blocks part of the detector viewing angle, and from -90° to 90° for θ_i in case of reflectance measurements.

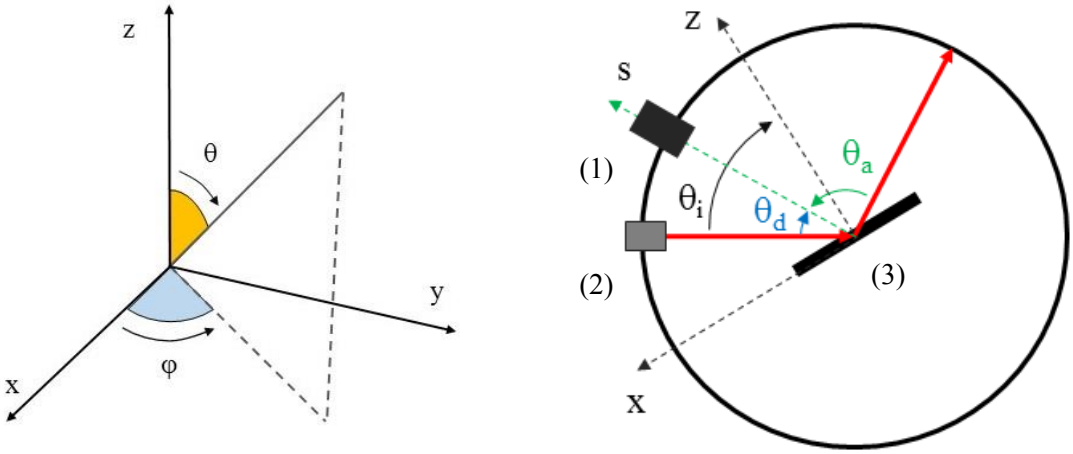

(a) (b)

Figure 1. Generic spherical coordinates (a), and top-view scheme of the ARTA with moving detector (1), beam periscope (2), and sample (3), (b).

2.3 Experimental setup

The measurements are carried out with a Perkin Elmer Lambda 950 double beam spectrophotometer equipped with the ARTA goniophotometer accessory by OMT Solutions BV, presented in [7] and shown in figure 2. The sample is positioned on a motorized rotation stage in the center, whereas the PMT and PbS sensors, mounted in a 25 mm integrating sphere with a 30 mm wide and 17 mm high entrance port, can rotate around the same axis as the sample holder.

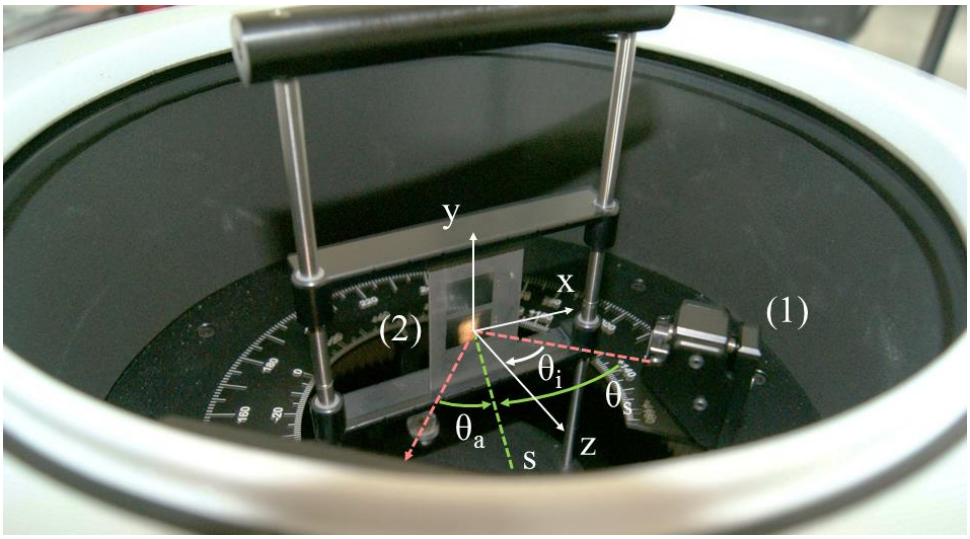

Figure 2. Sample compartment of the ARTA with illustrated axes and angles: sample beam periscope (1), sample with alignment beam (2).

The accessory has two polarizing filters, and every measurement is repeated twice, in *s* and *p* polarization, and results are then averaged. The beam size with normal incidence is 10 mm x 5 mm, and its width is increased with the sample rotation angle θ_i by the factor $1/\cos(\theta_i)$. The distance between the sample center and the entrance port is 91.5 mm. For this experimental campaign, the sample port width has been reduced to 14 mm with black paperboard in order to improve angular accuracy, giving the sensor a horizontal view angle $\Delta\theta_v = 8.8°$. The vertical view angle is $\Delta\varphi_v = 10.6°$. The errors introduced by using a finite sized detection solid angle in benchtop goniophotometers are well analyzed in [6], and they depend on both the aperture size and the variation of the measured radiation over the aperture, thus they can vary with the instrument setup, the measurement sample, and the sample properties. An in-depth discussion of these effect is beyond the purpose of this work, however it should be pointed out that measurement errors of about 3% are expected.

In this work, measurements are taken in the Vis-NIR wavelength range, i.e., from 350 to 2000 nm, with steps of 10 nm. A preliminary analysis has been carried out with an angle of incidence of incoming radiation $\theta_i = 45°$, and sensing angles θ_d ranging from 15° to 105° with 15° increments. Since very low reflected radiation values have been detected outside aspecular angles θ_a of ±15°, the main measurement campaign has been carried out with θ_a ranging from -15° to 15°, with 5° increments. Two angles of incidence, $\theta_i = 45°$ and $\theta_i = 15°$ are considered. The measurement geometries are listed in tables 1 and 2 and illustrated in figure 3.

Table 1. Preliminary test geometries

θ_i = 45°								
θ_d [°]	345	15	30	45	60	75	90	105
θ_a [°]	105	75	60	45	30	15	0	-15

Table 2. Test geometries

θ_i = 15°							
θ_d [°]	15	20	25	30	35	40	45
θ_a [°]	15	10	5	0	-5	-10	-15
θ_i = 45°							
θ_d [°]	75	80	85	90	95	100	105
θ_a [°]	15	10	5	0	-5	-10	-15

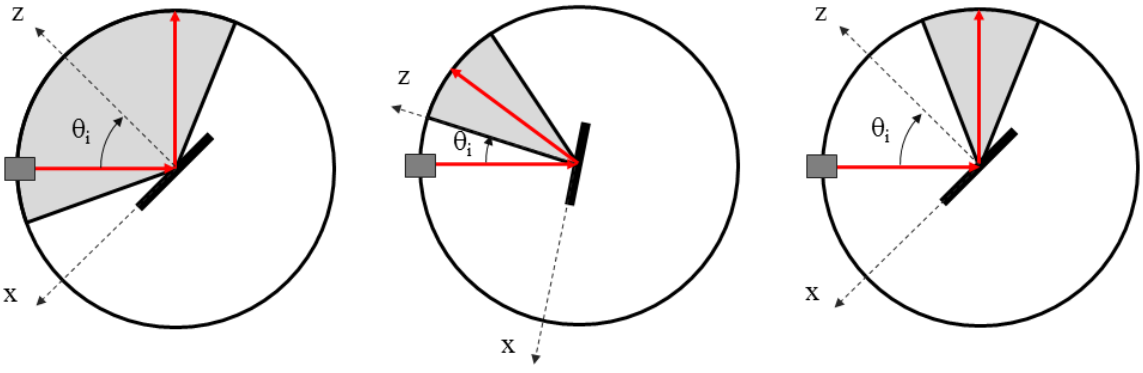

(a) (b) (c)

Figure 3. Scheme of the test geometries. Preliminary test (a), test with θ_i =15° (b), test with θ_i =45°. The highlighted (grey) region is swept by the detector with discrete angular intervals.

2.4 Samples

The samples are 0.5 mm thick steel plates with 16 mm x 12 mm surface polished areas, prepared with a pulsed active fiber laser source, operating at a wavelength of 1064 nm. The setup is fully presented in [8]. Four finishes are considered representing two different roughness classes and processing environments. Finishes N1A1 and N2A2 were obtained in Ar atmosphere, exhibiting low and high roughness classes respectively. Analogously, N1 and N2 were obtained under N_2, and represent low and high surface roughness cases. The different textures of the laser polished surfaces are highlighted in figure 4. The "untreated steel" measurements have been taken on the backside of the specimen with N1 and N2 treatments.

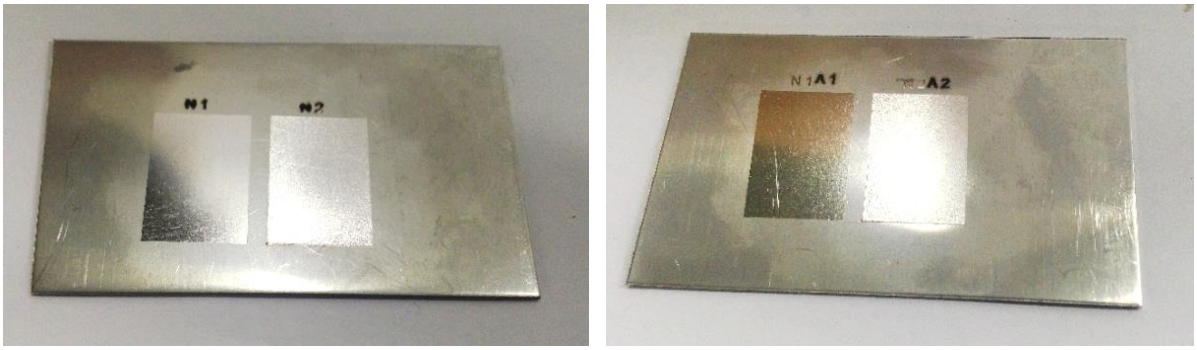

Figure 4. Pictures of the laser-treated samples.

3 Results

3.1 Angle of incidence effect

A slight increase of the specular component of the reflection with the increase of the angle of incidence θ_i from 15° to 45° is shown in figures 5 and 6. In particular, sample N1A1 shows lesser sensitivity to variations of θ_i than the other samples. It is common behavior between all samples that reflectance differences peak at the specular direction.

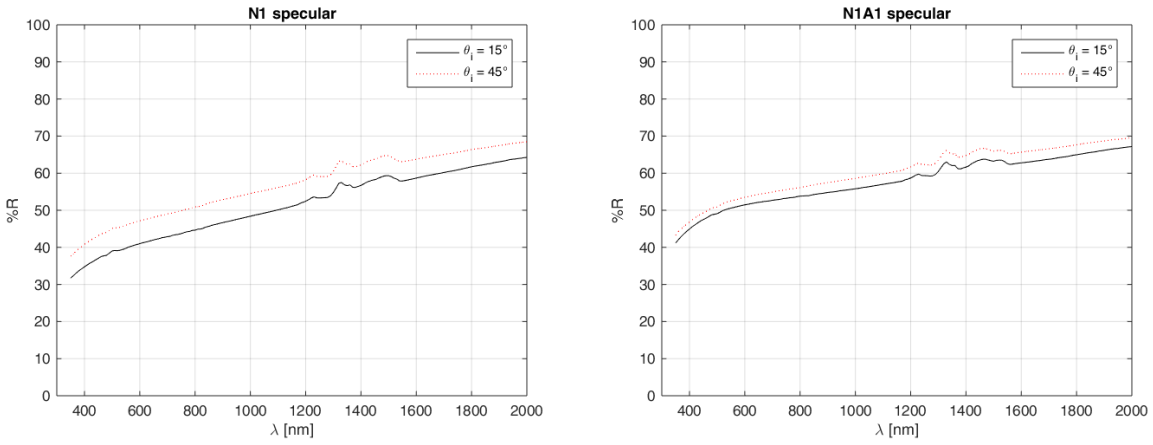

Figure 5. Spectra in specular directions, angle of incidence θ_i = 15° and θ_i = 45°, samples N1 and N1A1

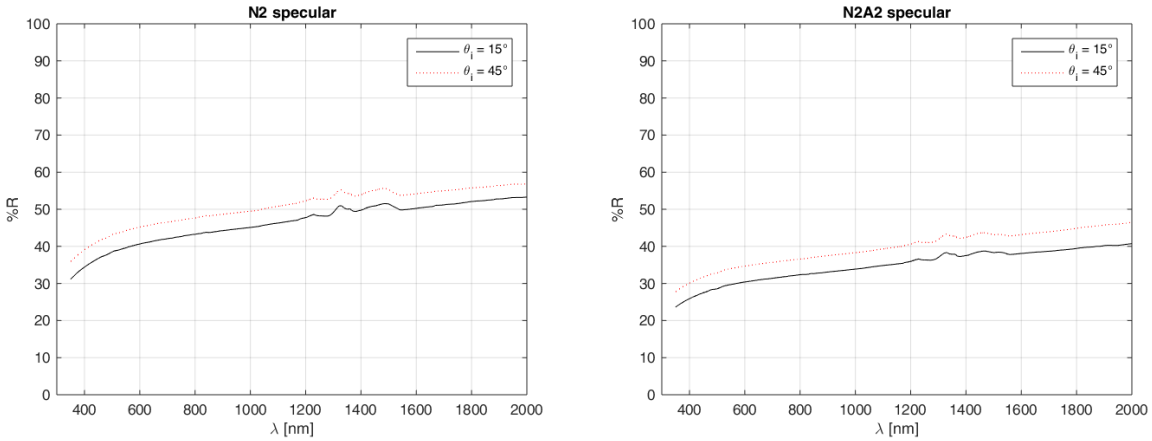

Figure 6. Spectra in specular directions, angle of incidence $\theta_i = 15°$ and $\theta_i = 45°$, samples N2 and N2A2

3.2 BRDF

The BRDFs of the laser-treated surfaces are shown for $\theta_i = 45°$ in figure 7. It should be noted that the four different finishes show different angular and spectral variations: sample N1 is the only one that presents high BRDF values for negative aspecular angles θ_a, whereas sample N1A1 shows a perfectly symmetric behavior. The peculiarity of sample N2A2 is that it's the only one whose BRDF doesn't peak at $\theta_a = 0°$.

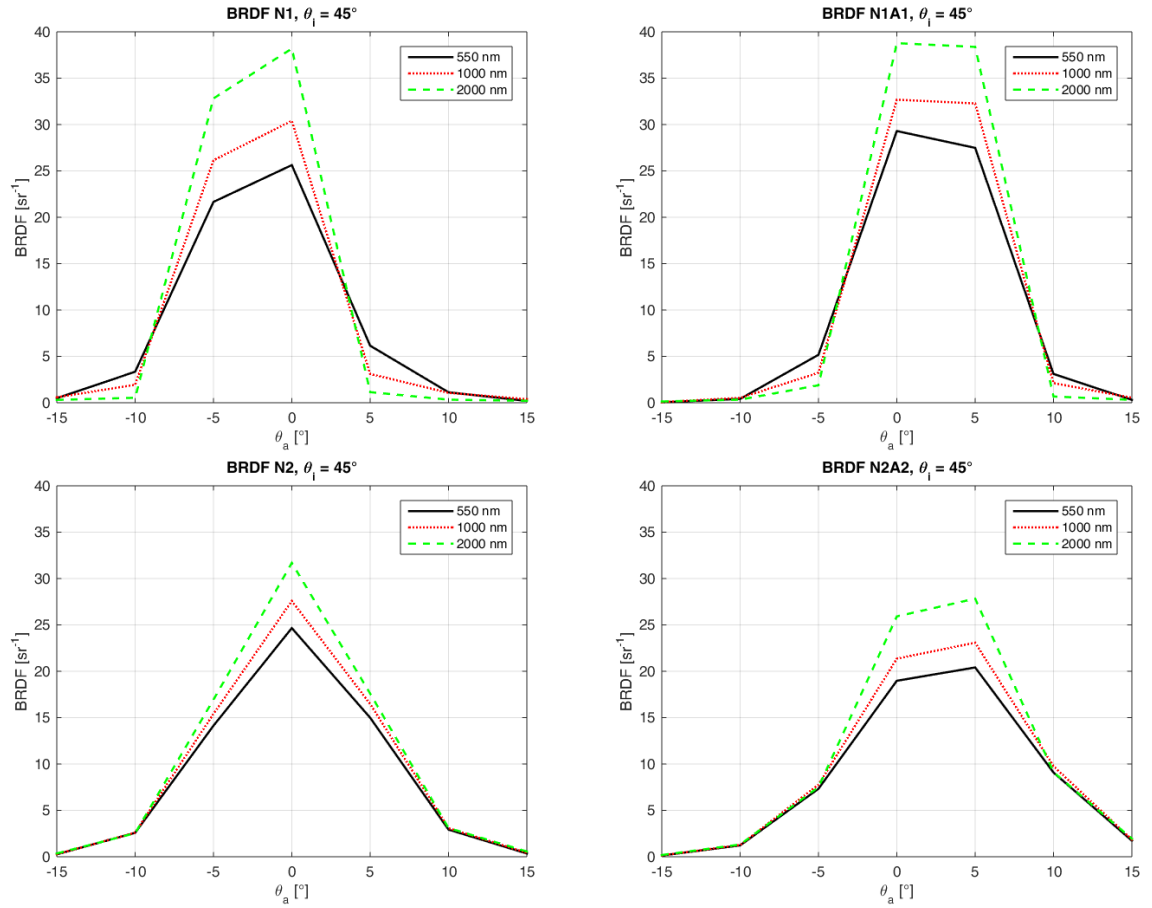

Figure 7. BRDF of the four laser-treated surfaces at three wavelegths, angle of incidence $\theta_i = 45°$.

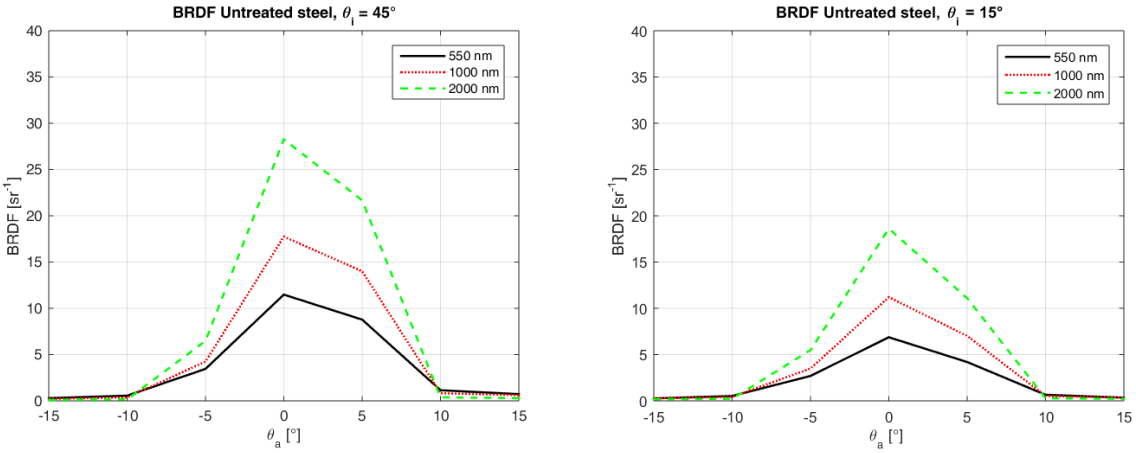

Figure 8. BRDF of the untreated steel surface at three wavelegths, angle of incidence θ_i = 45° (left) and θ_i = 15° (right).

The curves show similar trends for θ_i = 15°, as shown in figure 9, but with smaller values, and as pointed out in paragraph 3.1. The reflectance increase of the laser polished surfaces with respect to the untreated bare steel is easily noticeable in figure 8 by comparison. Further considerations on this point are drawn in section 3.3.

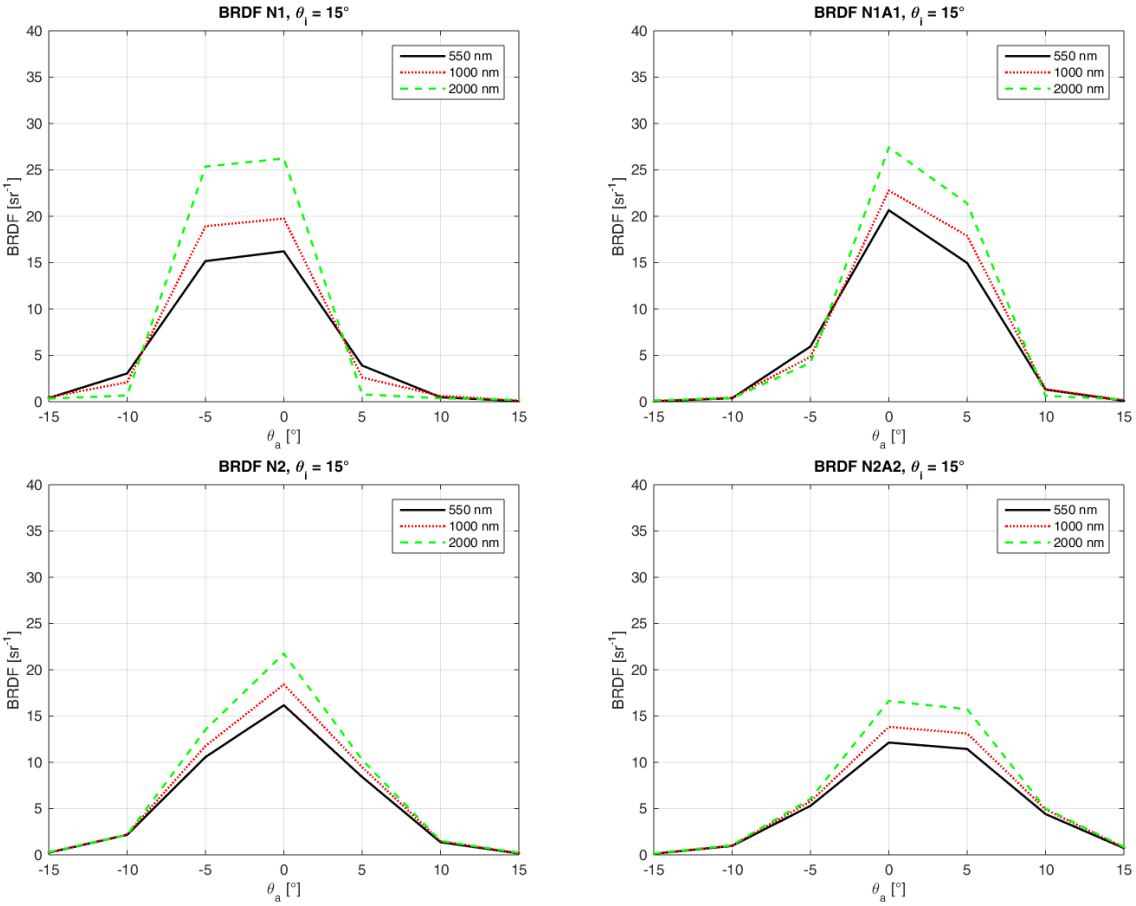

Figure 9. BRDF of the four laser-treated surfaces at three wavelegths, angle of incidence θ_i = 15°.

3.3 Reflectance differences

The surface polishing process causes an increase of the mirror-like behavior in steel, by factors listed in table 4, while considering the visible wavelength range. The largest specular reflectance increase is shown by sample N1A1, while the lowest by sample N2A2. However, the most interesting behavior is the change of the angular reflection properties, which are very specific for each of the four samples. Figure 10 shows, indeed, that the four angular shapes of reflectance increase peak at different angles. The only sample that also shows a reflection decrease, for $\theta_a = 5°$, is sample N1.

Table 3. Average reflectance increase in specular direction due to laser polishing, Vis range

	N1	N1A1	N2	N2A2
$\theta_i = 15°$ [%R]	22.7	32.9	22.2	12.2
$\theta_i = 45°$ [%R]	25.1	31.2	23.0	12.7

Figure 11 shows a 3D plot of the angular variation of the spectra with θ_a, where the differences in shape between the sample N1 and the untreated bare steel surface can be highlighted.

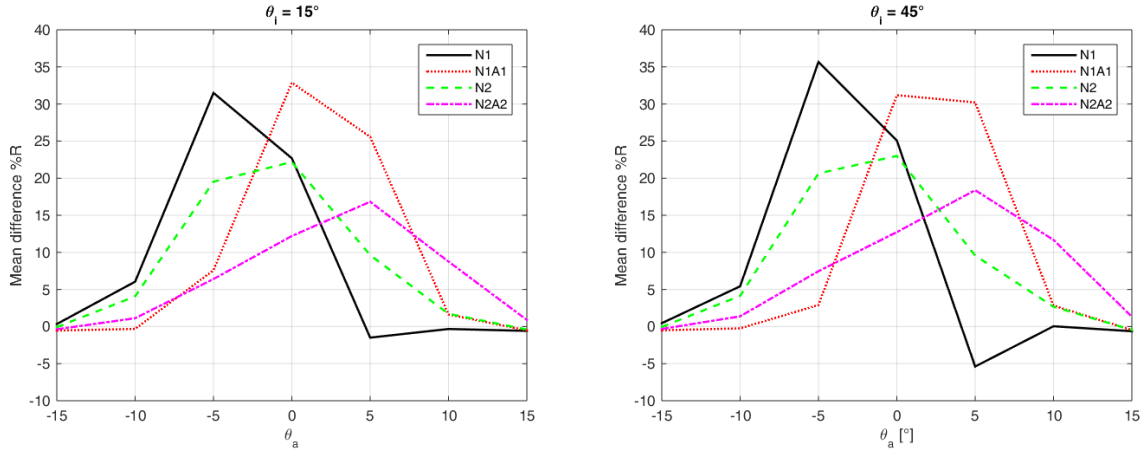

Figure 10. Average reflectance increase, Vis range, for $\theta_i = 15°$ and $\theta_i = 45°$, at seven aspecular angles.

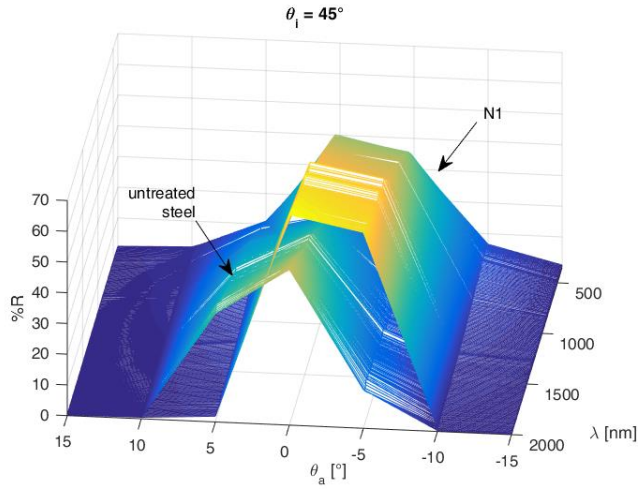

Figure 11. Full spectra with angular dependency of sample N1 and untreated steel, $\theta_i = 45°$

4 Conclusions

A first attempt to characterize the angular-dependent optical properties of steel laser polished surfaces has been carried out by means of the benchtop spectrogoniometer ARTA. The analyses allow to characterize the reflectance increase due to the laser machining. The BRDF has been calculated for two different angles of incidence, showing spectral and angular properties of the four considered samples. In addition, the results show that different machining parameters lead to different angular-dependent values of reflectance increase. Further studies are needed to verify the link between the angular and spectral variations of the surface reflectance, and the laser machining parameters, as well as the connection of spectral properties to the superficial roughness and texture.

Acknowledgments

The authors wish to thank prof. Barbara Previtali and dr. Ali Gökhan Demir of SITEC - Laboratory for Laser Applications of the Department of Mechanical Engineering at the Politecnico di Milano, to have provided the laser-treated samples analysed in this work.

References

[1] Maressa P, Anodio L, Bernasconi A, Demir A G and Previtali B 2014 *J of Adhes*. **91** 518-37
[2] Veiko V, Odintsova G, Ageev E, Karlagina Y, Loginov A, Skuratova A and Gorbunova E 2014 *Opt. Express* **22** 24342-7
[3] Bordatchev E V, Hafiz A M K and Tutunea-Fatan O R 2014 *Int. J. Adv. Manuf. Tech.* **73** 35-52
[4] Désage S F, Pitard G, Pillet M, Favrelière H, Maire J L, Frelin F, Samper S and Le Goïc G 2015 Extended visual appearance texture features *Proc. of SPIE* **9398**
[5] Nicodemus F E, Richmond J C, Hsia J J, Ginsberg I W and Limperis T 1977 *Geometrical Considerations and Nomenclature for Reflectance* (U.S. Dept. of Commerce, National Bureau of Standards)
[6] Johansson N, Neuman M, Andersson M and Edström P 2014 *App. Opt.* **53** 1212-20
[7] van Nijnatten P A 2003 *Thin Solid Films* **442** 74-9
[8] Franceschini F, Demir A G, Griffiths J D, Dowding C and Previtali B 2014 *Proc. of the 10th Conferenza del Colore (Genova, IT)* vol X B (Maggioli Editore) 20-31